Supporting Information

One-step synthesis of IrO$_x$ decorated ultrathin NiFe LDH nanosheets for efficient oxygen evolution reaction

Depei Liu[a,b], Yu Du[c], Taozhu Li[b], Hehe Zhang[d], Duanduan Liu[a,b], Weining Zhang[a,b], Huang Tang[b], Yanghui Hou[b], Jingsha Li[e], Shicheng Yan[*,b], Tao Yu[*, a], and Zhigang Zou[a,b]

[a] Jiangsu Key Laboratory for Nano Technology, National Laboratory of Solid State Microstructures, Collaborative Innovation Center of Advanced Microstructures, School of Physics, Nanjing University, Nanjing, 210093, P. R. China.

[b] Eco-materials and Renewable Energy Research Center (ERERC), College of Engineering and Applied Sciences, National Laboratory of Solid State Microstructures, School of Physics, Nanjing University, No. 22 Hankou Road, Nanjing, Jiangsu 210093, P. R. China
E-mail: yscfei@nju.edu.cn (S. Yan), yutao@nju.edu.cn (T. Yu)

[c] College of Chengxian, Southeast University, Nanjing, 210088, P. R. China.

[d] Department of Materials Science and Engineering, College of Materials, Xiamen University, Xiamen, Fujian 361005, P. R. China.

[e] Institute of Materials Science and Devices, Suzhou University of Science and Technology, Suzhou 215011, P.R. China

Experimental Section

Chemicals

Analytical reagents $Ni(NO_3)_2 \cdot 6H_2O$, $Fe(NO_3)_3 \cdot 9H_2O$, formamide, $NaNO_3$, NaOH, and KOH were purchased from Shanghai Chemical Reagent Co., Ltd (China). $IrCl_3$ was purchased from Meryer (Shanghai) Chemical Technology Co., Ltd (China). IrO_2 was purchased from Shanghai Macklin Biochemical Co., Ltd (China). All the above chemicals were used as received

Materials synthesis

A 20 mL aqueous solution contained 0.75 mmol $Ni(NO_3)_2 \cdot 6H_2O$, 0.25 mmol $Fe(NO_3)_3 \cdot 9H_2O$ and different amounts of $IrCl_3$ was added dropwise to a solution of 20.0 mL 0.01 M $NaNO_3$ containing 23 vol% formamide under magnetic stirring at 80 °C. Simultaneously, 0.25 M NaOH aqueous solution was added into the solution to maintain a pH of ~10. The reaction was completed within 10 min. The IrO_x decorated ultrathin NiFe LDH (IrO_x/U-NiFe-LDH) was collected by 8000 rpm centrifugation of 10 min and washed with DI water of more than 3 times, then kept in a gel state for subsequent use. For comparison, the synthesis of ultrathin NiFe-LDH (U-NiFe-LDH) was similar to that described above for IrO_x/U-NiFe-LDH, except the precursor solutions without $IrCl_3$. The bulk NiFe-LDH (Bulk-NiFe-LDH) was synthesized as the same without $IrCl_3$ and formamide. The IrO_x/C catalyst was perpared as the same method by using 1 mmol active carbon (Vulcan XC-72R) to replace $Ni(NO_3)_2 \cdot 6H_2O$ and $Fe(NO_3)_3 \cdot 9H_2O$.

Materials characterization

The as-prepared samples were characterized by X-ray diffraction (XRD, Rigaku Ultima III, Japan with CuKα radiation) for crystal structure analysis at 40 kV and 40 mA, X-ray photoelectron spectroscopy (XPS, PHI5000 Versa Probe, ULVAC-PHI, Japan) for composition and chemical states with monochromatized Al Kα excitation (The binding energies were corrected by normalizing the C1s spectrum at 284.6 eV, and a Shirley background was used for peak fitting), transmission electron microscope (TEM, FEI Talos F200s equipped with scanning TEM (STEM) for morphology and crystal lattice image, the energy dispersive spectroscopy (EDS) for composition analysis, and the atomic resolution high angle annular dark field (HAADF) images, atomic force microscope (AFM, Asylum Research, MFP-3D-SA, USA) for thickness of nanosheets and Zeta potential and particle size analyzer (ZetaPALS, Brookhaven, USA) for surface potential.

Electrochemical test

The OER catalytic performance was evaluated by linear sweep voltammetry (LSV), cyclic voltammetry (CV) and electrochemical impedance spectroscopy (EIS) on a CHI 660e bipotentiostation. To prepare the catalyst ink, 5 mg of catalyst and 1 mg of conductive carbon (Vulcan XC-72R) was dispersed in 950 μL ethanol by sonication for 20 min and then another ultrasonication after adding 50 μL Nafion (0.125 wt.%, DuPont). Next, 25 μL of ink was dropwise loaded on the carbon fiber paper (0.5 cm × 1 cm) with a microporous layer. After drying, the catalytic working electrode could be used for the electrochemical study. The geometric surface area of catalyst loaded on the carbon fiber paper is 0.5 cm^2, and the catalyst loading amount can be calculated as 0.25 mg cm^{-2}. Briefly, the above modified carbon fiber paper electrode as the working electrode, meanwhile an Ag/AgCl (Sat.) electrode and a Pt plate were used as reference and counter electrode, respectively. Before testing, the working electrodes were stabilized after 50 cycles CV treatment. LSV curves were tested in O_2-saturated 1.0 M KOH solution from 0 to 0.6 V (vs. Ag/AgCl) at a scan rate of 5 mV s^{-1} with inner resistance (IR) compensation (85 %). To evaluate the stability of as-prepared catalysts, the accelerated degradation

testing (ADT) was performed by LSV curves before and after 200, 400, 600, and 800 CV cycles. The EIS was tested in 1.0 M KOH solution by applying an AC voltage of 5 mV amplitude at the potential of 0.51 V (vs. Ag/AgCl) with frequency from 100 kHz to 0.1 Hz. Electrochemical active surface areas (ECSA) were measured by CV in the potential window 0 to 0.2 V (vs. Ag/AgCl) with different scan rates of 20, 40, 60, 80, 100, 120 and 140 mV s^{-1}. The current density at 0.1 V (vs. Ag/AgCl) was used for the calculation. The calculated equation of electrical double-layer capacitance (C_{dl}) is shown as:

$$C_{dl} = \frac{j_{nF}}{v} = \frac{j_a - j_c}{2v}$$

Wherein, j_{nF} is the non-Faraday current density, which equal to the half of difference between anodic current density (j_a) and cathodic current density (j_a). v is the scan rate. Thus, the C_{dl} is the slope of the fitting line for j_{nF} versus different scan rates.

The ECSA can be calculated by: $\mathrm{ECSA} = \frac{C_{dl}}{C_{dl,Ref}}$, the $C_{dl,Ref}$ is 0.04 mF cm^{-2} in the alkaline condition[1, 2].

The turnover frequency (TOF) was calculated by the equation:

$$\mathrm{TOF} = \frac{j \times A}{4 \times F \times n}$$

where j is the current density at 0.53 V or 0.58 V (vs. Ag/AgCl), A is the geometric surface area of the working electrode, F is the Faraday constant with a value of 96485 C mol^{-1}, and n is the mole number of the $Ni_3Fe(OH)_8NO_3$ for IrO_x/U-NiFe-LDH, U-NiFe-LDH, and Bulk-NiFe-LDH[3]. All initial potentials versus Ag/AgCl were standardized to potential versus reversible hydrogen electrode (RHE) by Nernst equation ($E_{RHE} = E_{Ag/AgCl} + 0.197 + 0.059pH$).
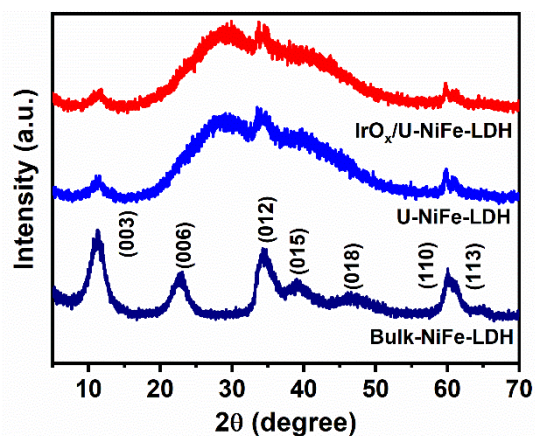
Fig. S1 XRD patterns of IrO$_x$/U-NiFe-LDH, U-NiFe-LDH, and Bulk-NiFe-LDH.

The pattern of Bulk-NiFe-LDH showed peaks at 11.3 °, 22.6 °, 34.4 °, 38.9 °, 46.6 °, 59.8 °, and 61.2 °, corresponding to (003), (006), (012), (015), (018), (110) and (113) facets of NiFe-LDH, respectively.[4] As for the patterns of IrO$_x$/U-NiFe-LDH and U-NiFe-LDH, the obvious peaks of (003), (012), (110) and (113) facets indicated that the addition of formamide could not impact the formation of NiFe-LDH species. Meanwhile, the peak of (003) facet was weak in both IrO$_x$/U-NiFe-LDH and U-NiFe-LDH, which proved that the NiFe-LDH planes are a few layers. Due to the gel state of IrO$_x$/U-NiFe-LDH and U-NiFe-LDH, a wide peak of them ranged at 20 ° ~30 ° represented the scatter of formamide.[5, 6] These facts demonstrated that the formamide could suppress NiFe-LDH layer stacking along the z-axis. Besides, the diffraction peaks of IrO$_x$ in the IrO$_x$/U-NiFe-LDH could not be observed. On the one hand, a few contents of IrO$_x$ leaded the weak intensity of related diffraction peaks, which were covered by other peaks. On the other hand, IrO$_x$ species were amorphous state or little clusters, which caused the inferior observability of related diffraction peaks.
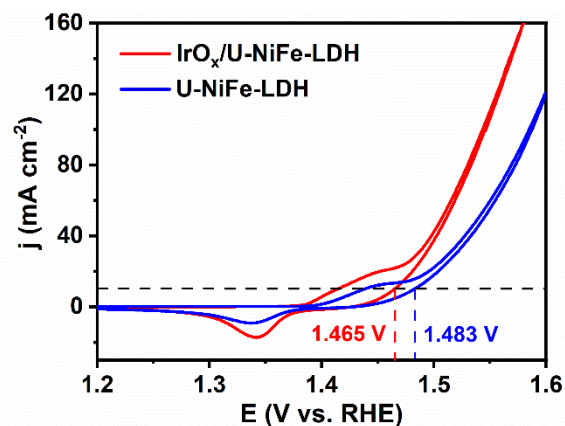
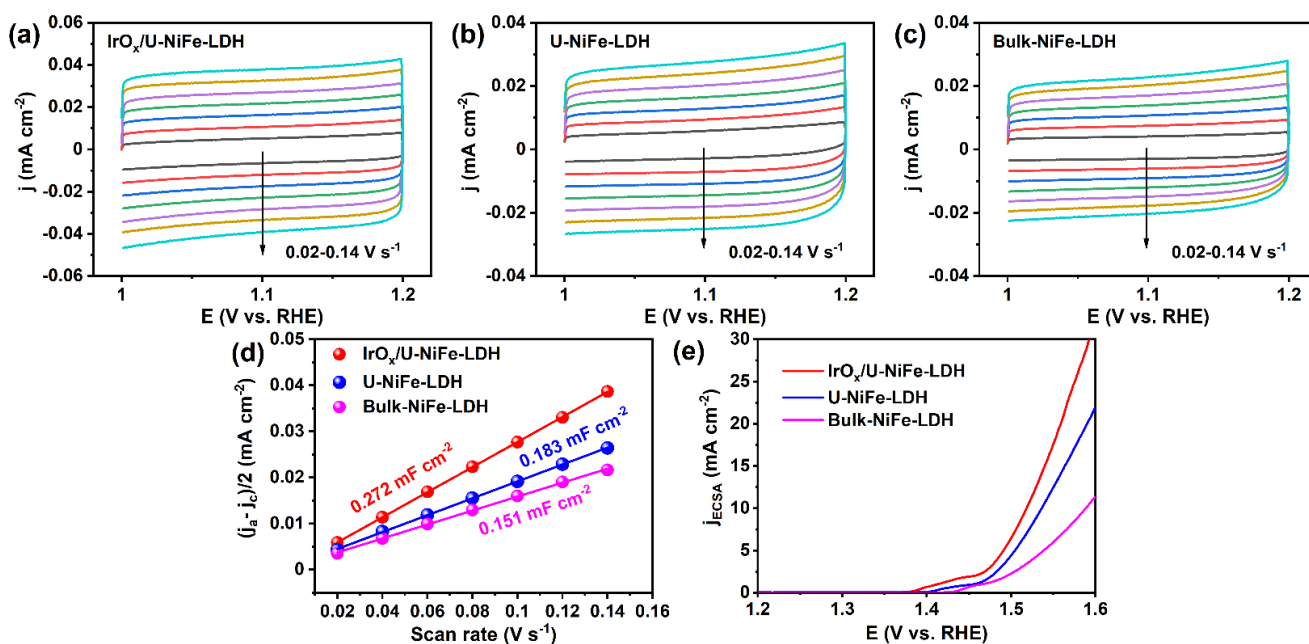**Fig. S2** CV curves of IrO$_x$/U-NiFe-LDH and U-NiFe-LDH.

Fig. S3 CV curves with different scan rates of (a) IrO$_x$/U-NiFe-LDH, (b) U-NiFe-LDH and (c) Bulk-NiFe-LDH. (d) the non-Faraday current density at 1.1 V versus different scan rates of as-prepared samples. (e) LSV curves of as-prepared samples that normalized to ECSA.
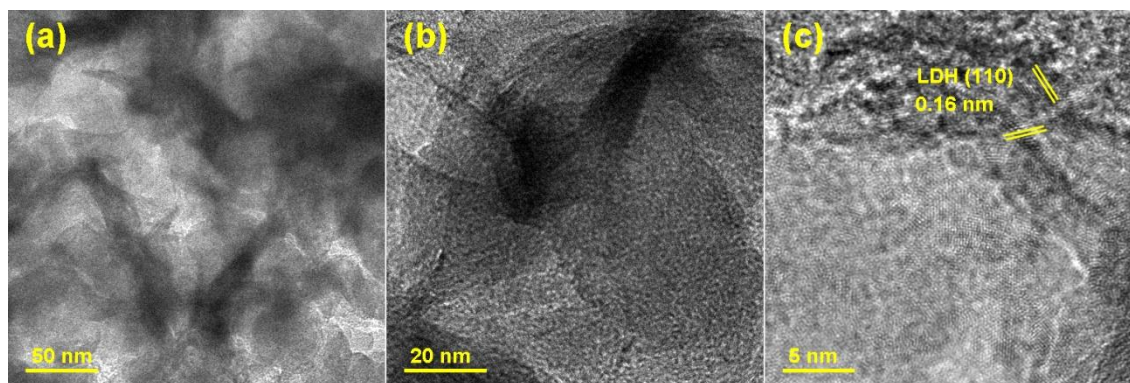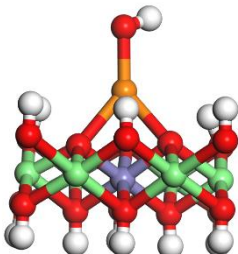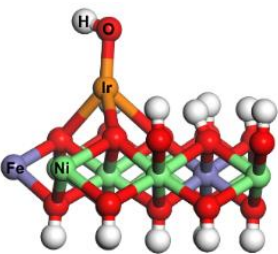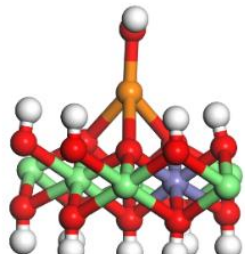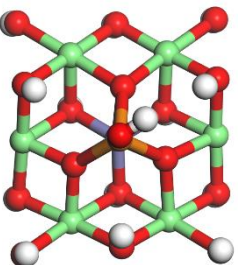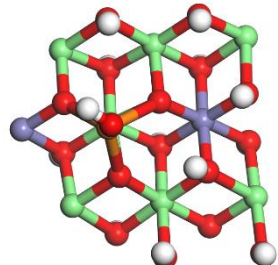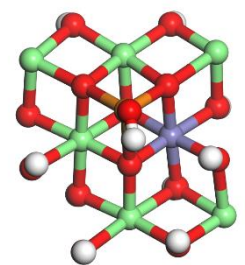

Fig. S4 (a, b) TEM images with different resolutions; (c) HRTEM image of IrO$_x$/U-NiFe-LDH after stability test.

Table S1 Relative energy and partial schematic diagram of IrO_x (Ir is orange) upon the Fe (blue), Ni (green), and O (red) sites for IrO_x/U-NiFe-LDH.

	Upon Fe site	Upon Ni site	Upon O site
Relative energy/eV	0	0.19	0.17
Side view			
Top view			

All DFT calculations were simulated with the DMol3 software package in Materials Studio. The exchange-correlation energy was described by the GGA function of the PBE, which was supplemented by the rotationally invariant "+U" description. The Hubbard U values were 3.8 eV for Ni 3d orbit and 4.3 eV for Fe 3d orbit. A Ni_3Fe-LDH crystal was built for further calculations. According to the AFM results (Fig. 1e, thickness of 1~2 nm), the structure of U-NiFe-LDH contained two $Ni_3Fe(OH)_8^+$ planes and one NO_3^- interlayer. Thus, the unit cell of U-NiFe-LDH had been built with a=6.09 Å, b=6.11 Å, c=7.28 Å and α=β=90 °, γ=120 °.[7] The (001) facet of U-NiFe-LDH was modeled by applying a (2×2) surface structure with a vacuum slab of 15 Å along the z-axis. The Brillouin zone was sampled using a grid of 4×4×1 Monkhorst-Pack type of k-points. The structure of IrO_x/U-NiFe-LDH was modeled by adding some IrO_x groups at the surface of the U-NiFe-LDH (001) facet. The structure optimization was based on an energy tolerence of $1×10^{-5}$ Ha, a force tolerence of 0.002 Ha/Å and a displacement tolerence of 0.005 Å. (1 Ha≈27.2114 eV)

Table S2 Comparison of OER activity for LDH-based catalysts at plane substrate.

Catalyst	Substrate	Overpotential at 10 mA cm^{-2}	Reference
IrO$_x$/U-NiFe-LDH	Carbon paper	236	This work
U-NiFe-LDH	Carbon paper	250	This work
Bulk-NiFe-LDH	Carbon paper	277	This work
^{s}Au/NiFe LDH[8]	Ti mesh	237	J. Am. Chem. Soc. 2018, 140: 3876–79.
Fe^{2+}-NiFe LDH colloid[9]	Carbon paper	249	Angew. Chem. 2018, 130: 9536–40.
Fe^{2+}-NiFe LDH array[9]	Carbon paper	195	Angew. Chem. 2018, 130: 9536–40.
3D NiFe-LDH HMS[10]	Carbon paper	290	J. Energy Chem. 2019, 33: 130–7.
Porous monolayer NiFe LDH[11]	Graphite paper	230	Adv. Energy Mater. 2019, 9: 1900881.
Ultrafine monolayer NiFe LDH[12]	Graphite paper	254	Adv. Energy Mater. 2018, 8: 1703585.
H$_2$PO$_2^-$/NiFe-LDH[13]	Carbon paper	215	Nano Res. 2017, 10: 1732–1739
Ni$_2$Fe-SDS-LDH[14]	Carbon paper	289	Electrochim. Acta 2017, 258: 554-60.
NiFe/RGO[15]	Glassy carbon	245	J. Power Sources 2015, 294: 437-43.
NiFe LDH nanosheets[16]	Glassy carbon	300	Nat. Commun. 2014, 5: 1-9.
NiCo-LDH nanoplates[17]	Carbon paper	307	Carbon 2016, 110: 1-7.
Ru/CoFe-LDHs[18]	Carbon paper	198	Nat. Commun. 2019, 10: 1-11.
ZnCo-LDH nanosheets[19]	Glassy carbon	385	J. Colloid Interf. Sci. 2020, 565: 351–59.

References

1. D. Voiry, M. Chhowalla, Y. Gogotsi, N. A. Kotov, Y. Li, R. M. Penner, R. E. Schaak and P. S. Weiss, *ACS Nano*, 2018, **12**, 9635-9638.

2. C. Zhang, W. Zhang, N. E. Drewett, X. Y. Wang, S. J. Yoo, H. X. Wang, T. Deng, J. G. Kim, H. Chen, K. K. Huang, S. H. Feng and W. T. Zheng, *ChemSusChem*, 2019, **12**, 1000-1010.

3. B. M. Hunter, W. Hieringer, J. R. Winkler, H. B. Gray and A. M. Müller, *Energy Environ. Sci.*, 2016, **9**, 1734-1743.

4. B. W. Zhang, C. Q. Zhu, Z. S. Wu, E. Stavitski, Y. H. Lui, T. H. Kim, H. Liu, L. Huang, X. Luan, L. Zhou, K. Jiang, W. Huang, S. Hu, H. Wang and J. S. Francisco, *Nano Lett.*, 2020, **20**, 136-144.

5. Q. Wang and D. O'Hare, *Chem. Rev.*, 2012, **112**, 4124-4155.

6. L. Li, R. Ma, Y. Ebina, N. Iyi and T. Sasaki, *Chem. Mater.*, 2005, **17**, 4386-4391.

7. Y. M. Bi, Z. Cai, D. J. Zhou, Y. Tian, Q. Zhang, Q. Zhang, Y. Kuang, Y. Li, X. Sun and X. Duan, *J Catal*, 2018, **358**, 100-107.

8. J. F. Zhang, J. Y. Liu, L. F. Xi, Y. F. Yu, N. Chen, S. H. Sun, W. C. Wang, K. M. Lange and B. Zhang, *J. Am. Chem. Soc.*, 2018, **140**, 3876-3879.

9. Z. Cai, D. J. Zhou, M. Y. Wang, S. M. Bak, Y. S. Wu, Z. S. Wu, Y. Tian, X. Y. Xiong, Y. P. Li, W. Liu, S. Siahrostami, Y. Kuang, X. Q. Yang, H. H. Duan, Z. X. Feng, H. L. Wang and X. M. Sun, *Angew. Chem. Int. Ed. Engl.*, 2018, **57**, 9392-9396.

10. H. H. Zhong, T. Y. Liu, S. W. Zhang, D. Li, P. Tang, N. Alonso-Vante and Y. Feng, *J Energy Chem*, 2019, **33**, 130-137.

11. X. Zhang, Y. F. Zhao, Y. X. Zhao, R. Shi, G. I. N. Waterhouse and T. R. Zhang, *Adv. Energy Mater.*, 2019, **9**, 1900881.

12. Y. F. Zhao, X. Zhang, X. D. Jia, G. I. N. Waterhouse, R. Shi, X. R. Zhang, F. Zhan, Y. Tao, L. Z. Wu, C. H. Tung, D. O'Hare and T. R. Zhang, *Adv. Energy Mater.*, 2018, **8**, 1703585.

13. M. Luo, Z. Cai, C. Wang, Y. M. Bi, L. Qian, Y. C. Hao, L. Li, Y. Kuang, Y. P. Li, X. D. Lei, Z. Y. Huo, W. Liu, H. L. Wang, X. M. Sun and X. Duan, *Nano Res.*, 2017, **10**, 1732-1739.

14. H. H. Zhong, X. K. Cheng, H. T. Xu, L. Li, D. Q. Li, P. G. Tang, N. Alonso-Vante and Y. J. Feng, *Electrochim. Acta*, 2017, **258**, 554-560.

15. D. H. Youn, Y. B. Park, J. Y. Kim, G. Magesh, Y. J. Jang and J. S. Lee, *J. Power Sources*, 2015, **294**, 437-443.

16. F. Song and X. L. Hu, *Nat. Commun.*, 2014, **5**, 4477.

17. C. Yu, Z. B. Liu, X. T. Han, H. W. Huang, C. T. Zhao, J. Yang and J. S. Qiu, *Carbon*, 2016, **110**, 1-7.

18. P. S. Li, M. Y. Wang, X. X. Duan, L. R. Zheng, X. P. Cheng, Y. F. Zhang, Y. Kuang, Y. P. Li, Q. Ma, Z. X. Feng, W. Liu and X. M. Sun, *Nat. Commun.*, 2019, **10**, 1711.

19. C. Y. Qiu, F. X. Cai, Y. Wang, Y. J. Liu, Q. X. Wang and C. Zhao, *J. Colloid Interface Sci.*, 2020, **565**, 351-359.